BR05 - Bauxite Residue Supported Ag Nanoparticles: A Highly Effective and Recyclable Catalyst for Hydrogenation of p-Nitrophenol

Meerambika Behera [1], Nitika Tiwari [2], Shirsendu Banerjee[3], Sankha Chakrabortty[4] and Suraj Tripathy[5]

1. PhD Student
2. PhD Student
3. Assistant Professor
4. Assistant Professor
5. Associate Professor

School of Chemical Technology, Kalinga Institute of Industrial Technology, Bhubaneswar, India

Corresponding author: suraj.tripathy@kiitbiotech.ac.in

Abstract

Heterogeneously catalyzed reactions are one of the most important chemical processes exploited for the production of a large number of modern-day products. They have been used extensively in petroleum cracking, fine chemicals synthesis, environmental remediation and synthetic chemistry. Owing to their substantially large surface area, sizeable assembly of active surface sites and the existence of quantum confinement effects, metallic nanostructures have been used as heterogamous catalysts for range reactions. However, unprotected metal nanoparticles are usually suffered from various technical limitations such as irreversible agglomeration, catalyst poisoning and limited life cycle. To overcome these technical drawbacks, catalysts are usually dispersed on chemically inert materials such as mesoporous Al_2O_3, ZrO_2 and ceramics, and these materials are expensive. In the current paper, efforts have been made to develop a low-cost alternative catalytic material using bauxite residue, which is abundantly available. Considering these aspects, in the present work, we report hydrogenation of p-nitrophenol to p-aminophenol on bauxite residue supported silver nanoparticles. Supported silver nanoparticles are synthesized by chemical impregnation of nanosized silver particles on bauxite residue via reduction/precipitation technique. Phase and crystal structure of synthesized materials have been investigated by XRD. FTIR spectroscopy was employed to analyze the presence of surface molecules on the resultant material. SEM/TEM was used to investigate the morphology of the supported catalysts. Synthesized material has shown higher catalytic performance than unprotected Ag nanoparticles. Our investigation revealed higher catalytic activity of the Bauxite residue supported silver nanoparticles with possible potential for future industrial applications.

Keywords: Bauxite residue, silver, catalysis, hydrogenation, p-nitrophenol.

1. Introduction

Bauxite Residue (BR) or red mud is the solid residue from alumina production in the Bayer process [1,2]. Approximately 2–3 tonnes of bauxite are needed to produce 1 tonne of alumina, so the amount of BR produced can be estimated by applying the ratio of 1.5 to alumina production data [3]. The global stock of BR was predicted to reach approximately 4 billion tons in 2019, with a production rate of 0.15 billion tonnes per year [4]. Around 2 tonnes of caustic insoluble residue known as 'Bauxite Residue' or 'Red Mud' is generated by the NALCO alumina refinery at Damanjodi, Orissa for every tonne of alumina produced.

Aluminium metal is produced from aluminium oxide phases that constitute between 38 to 60% of the bauxite ore. The balance of bauxite is made up of Fe_2O_3, SiO_2, TiO_2 and other minor oxide phases. After the dissolution of bauxite in caustic soda, these impurities remain suspended until

separated by settling after being washed and are then pumped as a slurry to the nearby Bauxite Residue Area (or Red Mud Pond).

BR poses environmental and disposal challenges. A major reduction in the quantity of BR deposited in storage areas is only possible through its utilization in one form or another. However, the inherent properties of BR poses difficulties for its bulk utilization. Prior to assessment of bulk utilization options for BR from the NALCO refinery, in-depth characterization is required. Rao et al. have reported the characteristics of sand residue from the NALCO refinery [5], but limited characterization of BR from this refinery has been published. BR has not been utilised in large quantities until now because of its alkalinity, technical and economic limitations, industrial conditions, public concerns about its potential health effects, and market demand [6]. The chemical and mineral composition of BR varies widely depending on the bauxite's origin and processing conditions, and consequently, no universal methods and standards are available for BR treatment [7,8].

BR storage areas occupy considerable land areas and may negatively impact local environments [9]. BR uses studied and applied to date include metal recovery, adsorbents, catalysts, building materials, and other applications [10].The BR utilization rate is less than 4% in China, so the majority of BR is left unutilized [11]. Although the safe disposal and storage of BR is an international issue and has been extensively researched, BR reuse appears a better alternative to the storage of BR and the risks it poses.

BR can be considered a valuable material instead of a waste due to its many potential reuse applications. The abundance of BR has led to extensive research into possible uses [12]. These include: recovery of Al, Fe, and rare earth metals [13,14]; a sorbent for treatment of contaminated water [15,16]; sequestration of CO_2 [17]; an additive to ceramics and building materials [18,19]; embankment construction [20]; and soil amendment [12,21–25], and all of these uses may play a role in reducing the storage of BR.

Noble metal nanoparticles (NPs) have received intensive attention in recent years, because of their fascinating physical and chemical properties that are considerably different from those of their bulk counterparts. In particular, nanoscaled metallic silver is of great research interest due to its high performance and relatively low cost in catalysis of a variety of chemical reactions [26–28]. For example, the reduction conversion of p-NP with borohydride catalyzed by Ag nano-catalyst to 4-aminophenol (p-AP) is of industrial and environmental importance. However, the practical use of Ag NPs is hindered by their severe aggregation during the catalytic process, unavoidably decreasing the active surface area, and degrading long-term of performance.

Considering the hazardous nature of p-NP, chemical industries are obliged to eliminate it from their effluent streams. Conventional methodologies for removal of p-NP from water such as coagulation, flocculation, ozonation, adsorption, and biological treatment are often chemically, energetically and operationally intensive, focused on small systems, and thus involve technical challenges during implementation and operation at large scale [29–34]. Catalytic reduction to amino-derivatives in the presence of suitable catalysts to eliminate the toxicity of p-NP is therefore considered one of the most preferred technologies.

In this context, this study reports a simple and fast catalytic reduction method for p-NP using bauxite residue with silver metal-based nanocomposite (NC), a novel material using BR with silver nanoparticles (Ag NPs). Using UV-Vis spectroscopy, the reduction of p-NP by BR@Ag NCs was measured at up to 99% in just ten minutes. Both materials are much cheaper than conventional metallic NPs and hence may find potential application as hydrogenation catalyst.

2. Materials and Methods

2.1 Materials

BR was collected from the NALCO alumina refinery. Trisodium citrate, sodium borohydride and silver perchlorate hydrate were purchased from SIGMA - ALDRICH, USA. All reagents and chemicals were used as received, and only distilled water (DW) was utilized for all the experiments.

2.2 Synthesis of BR

For this study, representative raw BR from the NALCO refinery was washed with distilled water (DW) at least 5 times. It was left overnight on the filter paper to dry in an oven at 80 °C. The dried BR was then ground in a mortar and pestle till a consistent smooth powder was achieved, followed by sonication for fifteen minutes. The powder was then weighed and stored in an airtight container.

2.3 Synthesis of BR@Ag NCs

A 50 mg sample of previously prepared BR was suspended in 97 mL of DW in a conical flask (CF) and sonicated for 15 min. The initial pH was recorded. After sonication, the CF was placed in an ice bath and stirred well until the temperature of the solution increased up to 4°C. Once the required temperature was attained, then 1 mL each of 3mM TSC, 1mM $AgClO_4$ and 100mM $NaBH_4$ was added sequentially with ten minutes between them. The solution was stirred vigorously at 600 rpm for 30 min and filtered using Whatman filter paper [1,2]. The brownish-orange product retained on the filter paper was dried overnight at 80 °C. The powder was removed and crushed well. The synthesized powder was weighed and kept in a desiccator [35,36].

2.4 Characterization of Catalysts

The bulk morphology of the NCs was investigated by scanning electron microscopy (SEM) and transmission electron microscopy (TEM). Energy dispersive spectroscopy (SEM-EDS, JSM-6510, JEOL, Japan) was used to identify the elements present in the NC system. Transmission electron microscopy (TEM) (Tecnai, G^2 20 Twin, FEI, USA) was employed to investigate the morphology of NC particles. Phase and crystal structure of the NC material at various calcination temperatures was studied by X-ray diffraction technique (XRD, Xpert Pro, Panalytical, Netherland). FTIR spectroscopy (Spectrum-GX, Perkin Elmer, USA) was utilized to understand surface functionality. The presence of organic impurities in the sample may affect the catalytic efficiency of the NCs at later stages.

2.5 Catalytic Reduction of p-NP

The catalytic activity of the prepared BR@Ag NCs was investigated using the reduction of p-NP to p-AP in the presence of excess $NaBH_4$ as a model reaction in a quartz cuvette and monitored by a UV/Vis spectrophotometer (Agilent,Cary 100) [37,38]. Briefly, the reaction procedure is as follows: 0.2 mM p-NP and 15 mM freshly prepared ice-cooled aqueous solution of $NaBH_4$ were steadily mixed in a 1ml quartz cuvette. The solution changed from colourless to bright yellow instantly followed by the addition of different concentrations of BR@Ag (50, 100, 150, 200, 250 ppm) into the solution. Following this, UV-Vis spectra of the solution (scanning range of 200-800 nm) were recorded every 1 min. Considering the initial reaction time as t=0, a total of 10 min was required for the completion of the reaction, identified as a clear and colourless solution inside the cuvette. To interpret the repercussions of $NaBH_4$ on catalytic reaction, even different control

reactions were also carried out. The catalytic conversion efficiency of p-NP to p-AP in the reaction process could be calculated using the formula:

$$conversion\ efficiency\ of\ p\text{-}NP\ \% = \frac{C_0 - C_t}{C_0} \times 100 \quad (1)$$

Where C_t is the concentration of p-AP measured at time 't', and
C_0 is the initial concentration of p-AP measured at time zero.

Here, the measured conversion efficiency of p-NP to p-AP is calculated as ≈99%.

3. Results and Discussion

3.1 Catalytic Reduction of p-NP

Catalysis is the process of increasing the rate of a chemical reaction by adding a substance (the 'catalyst'), which is not consumed by the catalysed reaction and can continue to act repeatedly [39]. Interventions in the transfer of electrons from a donor molecule to an acceptor p-NP are done by the metallic NPs to catalyse the reaction process. Different heterogeneous catalysts are widely used and preferred in fine chemical industries considering their environmental compatibility. Specific active sites present on these heterogenous catalysts gives an advantage in increasing the process efficiency compared to that of metallic NPs. This tendency is supported by access to novel catalytic materials and contemporary methods of placing specific active sites onto catalyst surfaces. From this perspective, BR@Ag NCs could be a suitable candidate for the degradation of different organic pollutants, such as p-NP. Table 1 displays the ranges for common BR elemental constituents, although the values vary widely [40,41].

Table 1. Typical ranges of BR elemental composition.

Elemental Oxide	Percentage composition
Fe_2O_3	5-60%
Al_2O_3	5-30%
TiO_2	0-15%
CaO	2-14%
SiO_2	3-50%
Na_2O	1-10%

To understand the catalytic properties of BR@Ag NCs, the degradation of p-NP to p-AP by the NCs was examined. This degradation was in the presence of $NaBH_4$, which serves as a reducing agent as well as a source of hydrogen for the catalytic reaction. The experiment was performed spectrophotometrically in a UV-Vis spectrometer [42,43]. The total reaction procedure was performed in a 1 mL quartz cuvette. The injection of different chemical reagents follows this sequence: (i) distilled water (ii) BR@Ag (iii) 4-NP (iv) $NaBH_4$. Before loading the catalyst, it was sonicated for 15 mins and was maintained uniformly at room temperature (298 K) to avoid any agglomeration.

An aqueous solution of $NaBH_4$ and p-NP displayed a clear peak at 400 nm. Upon adding $NaBH_4$, the colourless solution of p-NP instantly turned a vivid yellow. The movement of peaks from 400 nm to 300 nm of p-NP to p-AP respectively could be attributed to the formation of colourless p-

aminophenolate ions from pale-yellow coloured p-nitrophenolate ions [44]. Both the peaks were visible during the reaction, allowing the quantification of the ongoing p-NP to p-AP conversion.

The high performance of this catalyst may be related to the optimum size of BR@Ag, not only limited to its pores or apertures, but also to the external surface, as well as the high loading of $NaBH_4$. The distinctive morphology of the catalyst facilitates reactant molecules' access to the catalytically active sites of BR@Ag NCs, resulting in the efficient catalytic reduction. The shape and peak positions of the product UV-Vis spectrum perfectly matches that of p-AP [37,42,45,46]. The reaction was complete within 10 mins after charging with 150 ppm of BR@Ag nano-catalyst at room temperature (298 K). Completion was determined by the colour change of reaction mixture in the quartz cuvette from yellow to colourless, along with the quantitative yield of the final product, as measured by absorption at 300nm in the UV-Vis spectra.

No appreciable colour change occurred in either BR or Ag nanoparticle. In the 'control' case, when only p-NP and $NaBH_4$ were added, there was no significant colour change in the cuvettes, indicating that without a prior stimulator (which acts as a chemical reaction accelerator) there can be minimal or zero contact interaction between nitroarenes and the hydride ions present. Equal distribution and loading of the catalyst and reactant molecules is also required. On completion of the reaction, the catalyst was separated and washed with DW. The results show that BR@Ag NC was able to properly catalyze the reaction.

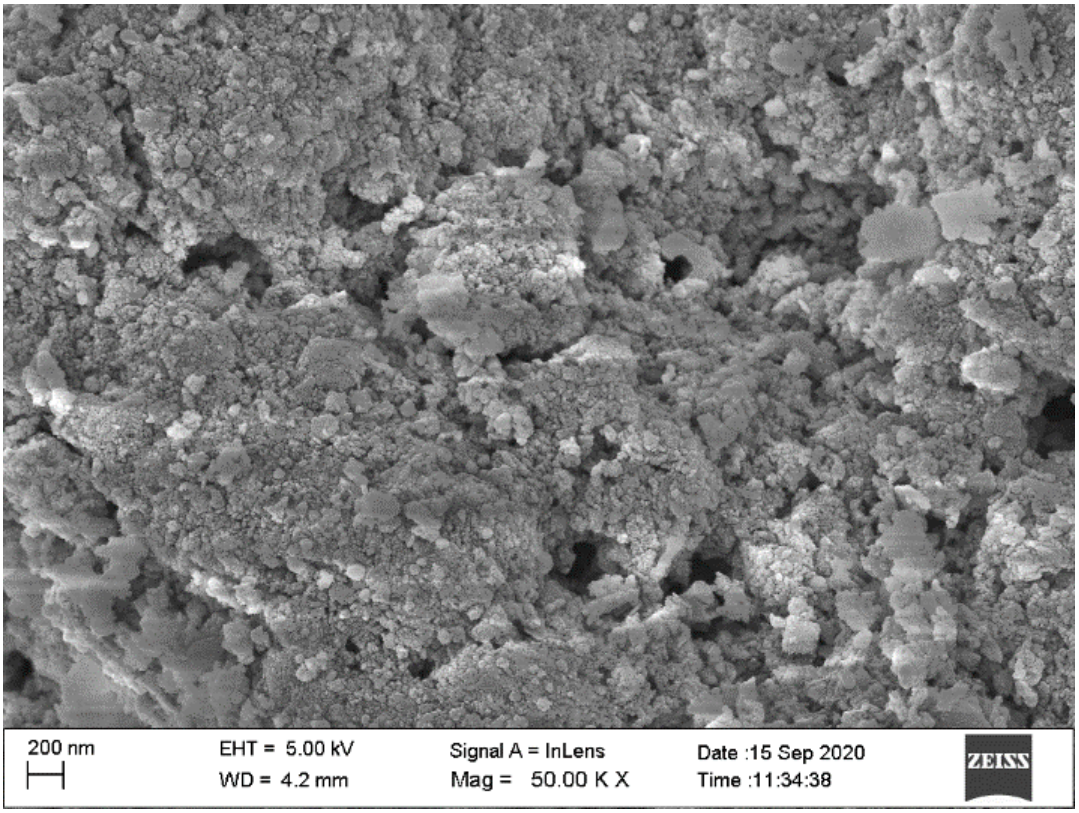

Figure 1. SEM-EDS image of BR@Ag NCs.

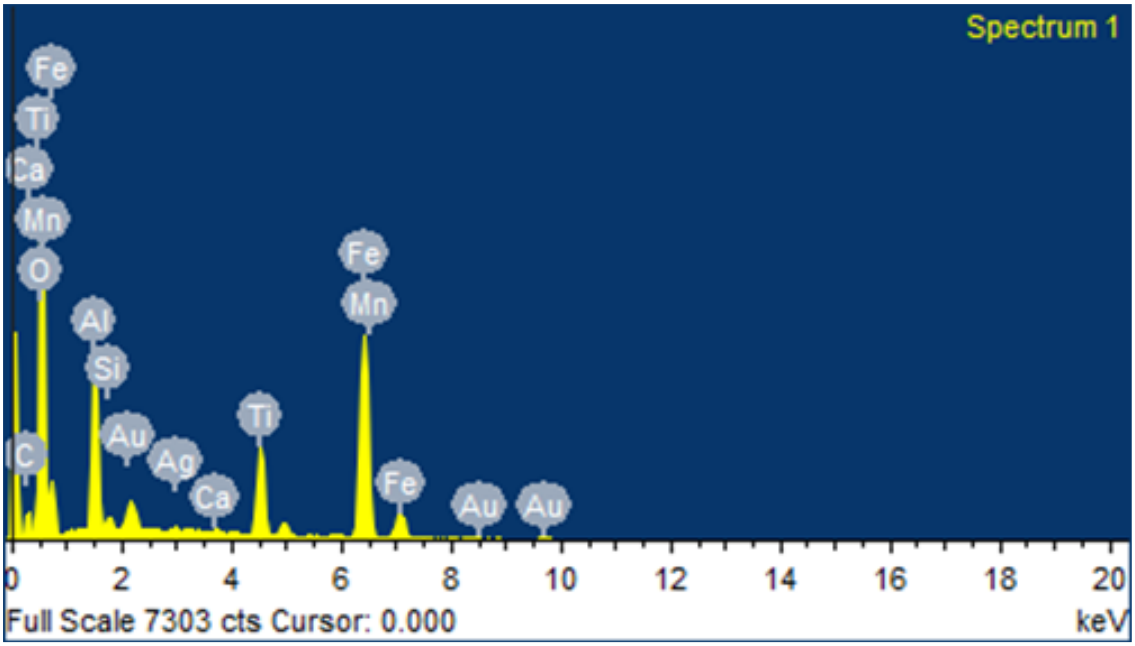

Figure 2. SEM-EDS spectra of BR@Ag NCs.

In the case of the control reactions, the peak intensity at λ_{max}= 400 nm remained unaltered in the absence of BR@Ag, indicating the absence of p-AP formation. The initial solution colour was also retained, verifying the absence of p-AP. Evolution of any corresponding peaks in the spectrophotometer was not observed when only BR@Ag was added, suggesting neither $NaBH_4$ nor BR@Ag NCs can act as an independent reductant in the whole reaction scheme. However, addition of only BR nanoparticles and $NaBH_4$ separately in the p-NP reaction mixture resulted in a zero reduction. An explanation for this observation may be that iron oxide in the BR (Fe_2O_3: 5-60 %) can act in the conversion of some of the BR to an amorphous Fe-B alloy while reacting with $NaBH_4$. As a result, BR NPs divide into micron size metallic-Fe nodules, ultimately causing the active pores on its surface to become and remain inaccessible for this chemical transformation [47].

The degradation of p-NP using Ag NPs has been already reported in the literature [26,48]. This was demonstrated in the high catalytic activity and the reducing properties of the BR@Ag and $NaBH_4$ respectively, seen in these results. The successful adsorption of p-NP or the reacting species onto the catalyst seems to be demonstrated by the production of p-AP within a short 10 mins period. The success of BR@Ag NCs in transforming p-NP to p-AP could be due to optimal particle size, maximum catalytic active sites, suitable porosity and/or the highly adsorbent nature of the catalyst.

TheSEM image of BR@Ag NCs has been shown with its respective EDS data in Figure 1 and 2 respectively. The image infers a uniform network exist in the components of BR with silver NPs. The synthesized BR@Ag NCs has an irregular surface and a non-spherical shape which may be due to agglomeration of particles. From the EDS spectra, we confirmed the presence of Ag NPs in the BR matrix where the weight percentage of Fe, Al, Ti, Ag and O in BR@Ag NCs was noted as 32.16, 7.83, 7.17, 0.043 and 40.64% respectively. This indicates the proper composite formation of Ag NPs on BR which resulted in the reduction of the reactant.

3.2 Proposed Mechanism

In this study, the reductant ($NaBH_4$) concentration greatly exceeded (300 times) that of p-NP. An explanation of the catalytic process might start with an electron transfer in form of hydride ion

from the donor ($NaBH_4$) to the acceptor compound (p-NP). As the borohydride anion is adsorbed on BR@Ag NCs surfaces, transfer of hydride ions occurs one by one from $NaBH_4$ and reduces p-NP molecules to form p-AP through intermediate compounds. The evolution of tiny hydrogen bubbles during the reaction reinforces the reduction reaction by stirring the solution. It is obvious that without a metallic catalyst, the initiating electron transfer step would be very slow, or in this case, might not proceed at all. It has been proposed that the rate of electron transfer occurring at the catalyst surface might be controlled through the following steps [49,50]:

1. Adsorption of p-NP molecules and $NaBH_4$ ions on BR@Ag surfaces.
2. Interfacial electron transport, promoting instantaneous intermediate phenolate ions formation.
3. Final desorption of p-Aminophenol from the catalyst surface.

From an application point of view, it is important to understand the effect of catalyst concentration to optimize catalyst concentration. Figure 3 shows the reduction of p-NP while varying the amount of BR@Ag NCs. Of the five concentrations added BR@Ag (50, 100, 150, 200, 250 ppm), 150 ppm resulted in conversion to p-AP in the shortest time, although it appears to the optimum, all concentrations of BR@Ag NCs converted all p-NP in approximately 15 mins. In this case, higher priority is given on the specific amount of the catalyst as every concentration taken are able to degrade p-NP successfully. However, the timing factor plays a great role here where the optimized concentration degrades p-NP in 10 mins (other concentrations do in 15 min) can be attributed to the fact that at this particular concentration (150 ppm) there might be uniform interaction and proper channeling of electrons between catalyst- p-NP- $NaBH_4$ molecules which accelerates the degradation time in shorter span.

Besides, the experiment was performed at different concentrations of p-NP as shown in Figure 4, and the optimal concentration obtained was 0.1mM. It was observed that the degradation took longer for a 0.05mM concentration of p-NP. On the other hand, the 0.25mM p-NP case did not result in significant conversion and was similar to the controlled reaction (without BR@Ag NCs). In general (assuming all the factors are constant) as reactant concentration increases, there is a proportional increase in the reaction rate. In order to convert p-NP into p-AP, the catalyst BR@Ag NCs should first bind with p-NP. This is usually achieved simply by random collisions between the p-NP molecules and BR@Ag NCs as these particles diffuse around in solution. Having said that, as the p-NP concentration increases from lower levels the rate of the reaction increases, but the degree to which the rate increases become progressively less and less as more BR@Ag NCs are occupied in form of BR@Ag–p-NP complexes. Eventually, saturation of the catalyst is achieved, and no further catalytic degradation will occur with increasing p-NP concentration.

In the control case where there is no BR@Ag catalyst, an almost a constant line having A_t/A_0 value ≈1 signifies that $NaBH_4$ alone in the absence of the catalyst is a weak reducing agent. It does not reduce p-NP without a substrate to facilitate adsorption and electron transfer simultaneously. Complete p-NP degradation took place in just 10 mins with 50 and 100 ppm of catalyst.

With this understanding of the reaction mechanism, it is interesting to compare the BR@Ag catalyst's productivity with that of the individual BR@Ag components (BR and Ag) as catalysts. Figure 5, presents an optimized amount the nano-catalysts BR@Ag, BR and Ag. As they all have a different structural morphology, they can present different catalytically active sites at their surface. The results reveal that, of the 3 catalysts, efficient reduction of p-NP is only achieved with BR@Ag NCs within a 15 min timeframe. BR and Ag by themselves appear not to provide any significant catalytic activity.

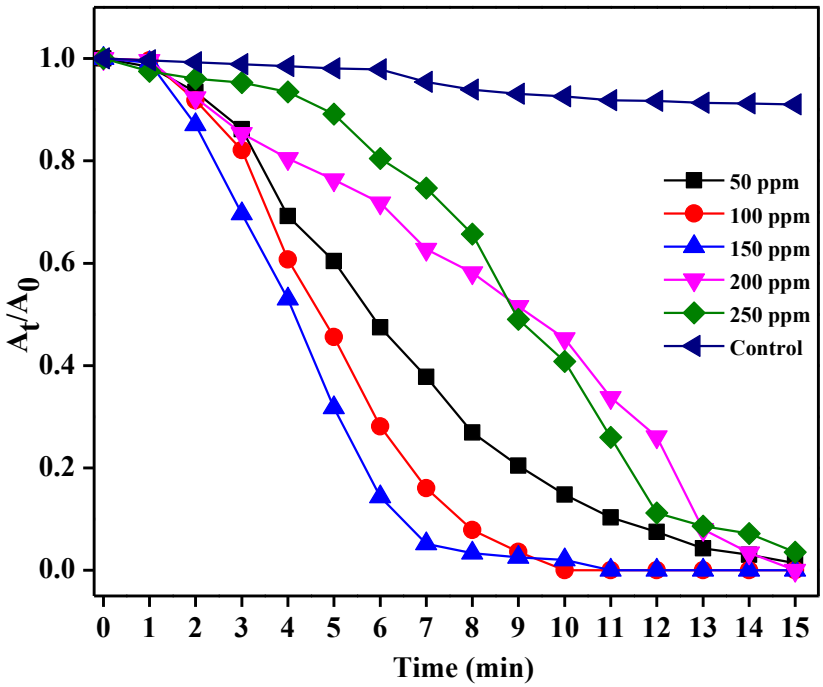

Figure 3. UV/Vis kinetic data for the catalytic reduction of p-NP using different BR@Ag NC concentrations. Control case is $NaBH_4$ added in the absence of catalyst.

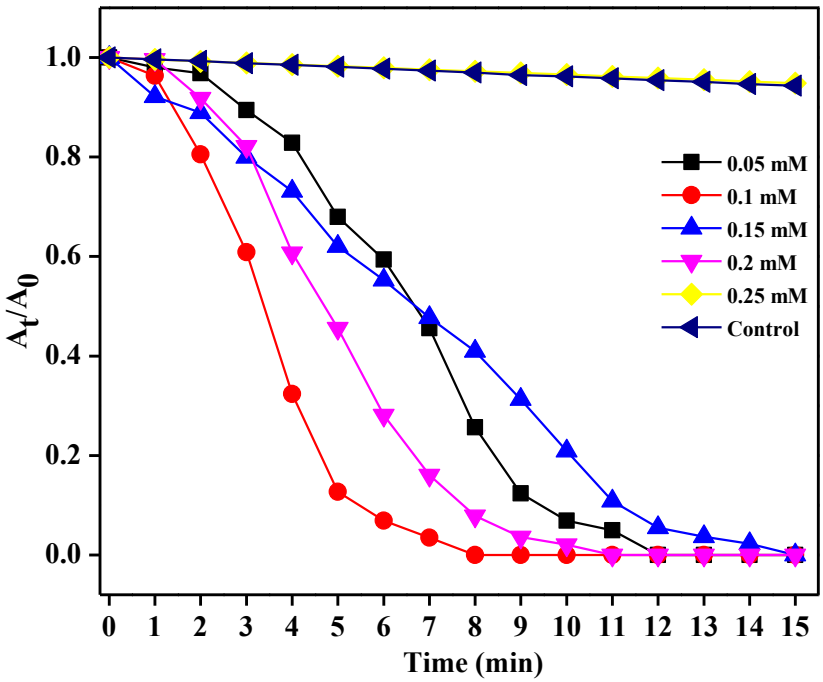

Figure 4. UV/Vis kinetic data for the catalytic reduction of p-NP at different p-NP concentrations. Control case is BR@Ag NCs in the absence of $NaBH_4$.

The absorbance value ($A_t/A_0 \approx 1$) of both BR and Ag NPs indicates agglomeration of these materials due to an increase in their inter-particle size post reaction. It is possible that this is because BR and Ag NPs are not well distributed in the p-NP solution, possibly exacerbated by the low catalytic degradation of p-NP.

The prepared BR@Ag NCs has numerous advantages:

- p-NP gets easy access to the active catalytic sites,
- the supported catalyst can be easily retrieved from the mixture at the end of reaction by simple centrifugation and lastly,
- possibility of top-bottom up-scaling and feasible industrial utilization can smoothly occur.

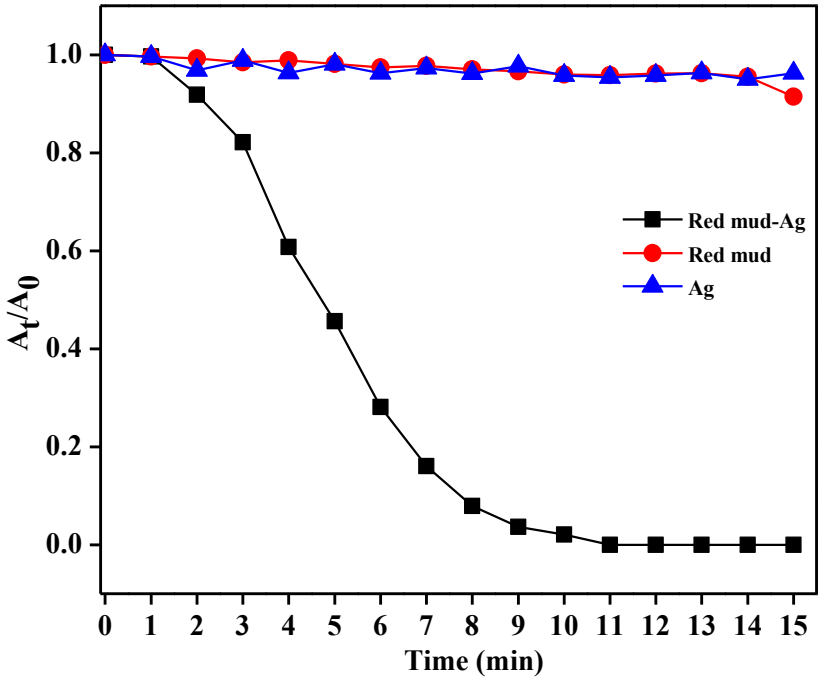

Figure 5. UV/Vis kinetic data for the catalytic reduction of p-NP using optimized concentration of different catalysts i.e., 150ppm.

4. Conclusions

In this study, an BR@Ag nanocomposite was prepared by facile sol-gel method and used as an efficient and stable heterogeneous catalyst for the reduction of p-NP. This NC exhibits high catalytic efficiency with 99% of p-NP reduced within 10 mins. The major advantages of BR@Ag NC include it being non-toxic, low cost and reusable. SEM-EDS suggested the presence of Ag NPs on the BR matrix. The optimal conditions found were a catalyst dosage of 150 ppm, p-NP concentration of 0.1 mM, which give a total reaction time of about 10 mins. Due to its high stability and renewable nature, BR@Ag NCs have been demonstrated as an efficient candidate for p-NP degradation.

5. References

1. X. Wang et al., Dealkalization of Red Mud by Carbide Slag and Flue Gas, *CLEAN-Soil, Air, Water*, Vol. 46, (2018), 600-634.
2. F. Lyu et al., Preliminary assessment of revegetation potential through ryegrass growing on bauxite residue, Journal of Central South University, Vol. 26, (2019), 404-409.
3. Y. Guo et al., Novel Process for Alumina Extraction via the Coupling Treatment of Coal Gangue and Bauxite Red Mud, *Industrial & Engineering Chemistry Research*, Vol. 53, (2014), 4518-4521.
4. F. Lyu et al., Utilisation of propyl gallate as a novel selective collector for diaspore flotation, *Minerals Engineering*, Vol. 131, (2019), 66-72.
5. L. Rao, Characterisation of sand rejects- A case study from an Alumina Refinery Plant, *Geology*, Vol. 2, (1997), 164-172.
6. L. Wang et al., Application of Red Mud in Wastewater Treatment, *Minerals*, Vol. 9, (2019), 281.
7. Hindalco becomes first ever company to achieve 100% red mud utilization worldwide, *Aluminium International Today*, https://aluminiumtoday.com/news/hindalco-becomes-1st-first-ever-company-to-achieve-100-red-mud-utilisation-worldwide/ (accessed on 16 October 2020).
8. E. Balomenos et al., A novel Red Mud Treatment Process: Process design and preliminary results, *TRAVAUX*, Vol. 36, (2011), 255-266.
9. E. Capehart, A Hekmat and R Singhal, *Proceedings of the 18th Symposium on Environmental Issues and Waste Management in Energy and Mineral Production*, 1st Edition, 2019, 267 pages.
10. S. Mustapha et al., Application of TiO_2 and ZnO nanoparticles immobilized on clay in wastewater treatment: a review, *Applied Water Science*, Vol. 10, (2020), 49.
11. A. Gelencsér et al., The Red Mud Accident in Ajka (Hungary): Characterization and Potential Health Effects of Fugitive Dust, *Environmental Science & Technology*, Vol. 45, (2011), 1608-1615.
12. C.L. Lockwood et al., Mobilisation of arsenic from bauxite residue (red mud) affected soils: Effect of pH and redox conditions, *Applied Geochemistry*, Vol. 51, (2014), 268-277.
13. B. Zhouet et al., Recovery of Alkali from Bayer Red Mud Using CaO and /or MgO, *Minerals*, Vol. 9. (2019), 269.
14. K.S. Hatzilyberis et al., Pilot-Plant Investigation of the Leaching Process for the Recovery of Scandium from Red Mud, *Industrial & Engineering Chemistry Research*, Vol. 41, (2002), 5794-5801.
15. S. Ju et al., Removal of cadmium from aqueous solutions using red mud granulated with cement, *Transactions of Nonferrous Metals Society of China*, Vol 22, (2012), 3140-3146.
16. I. Smičiklas et al., Effect of acid treatment on red mud properties with implications on Ni (II) sorption and stability, *Chemical Engineering and Journal*, Vol. 242, (2014), 27-35.
17. V.S. Yadav et al., Sequesteration of carbon dioxde (CO_2) using red mud, *Journal of Hazardous Materials*, Vol. 176, (2010), 1044-1050.
18. V. Sglavo et al., Bauxite 'red mud' in the ceramic industry. Part 2. Production of clay-based ceramics, *Journal of the European Ceramic Society*, Vol. 20, (2000), 245-252.
19. P.E. Tsakiridis, SA Leonardou and P Oustadakis, Red mud addition in the raw meal fir the production of Portland cement clinker, *Journal of Hazardous Materials*, Vol. 116, (2004), 103-110.
20. F. Kehagia, Construction of an unpaved road using industrial by-products (bauxite residue), *Proceedings of WSEAS TRANSACTIONS on ENVIRONMENT and DEVELOPMENT*, Vol. 10, (2014).
21. C. Klauber, M Gräfe, G Power, Bauxite residue issues: II (options for residue utilization), *Hydrometallurgy*, Vol. 108, (2011),11–32.

22. I.R. Phillips, Use of Soil Amendments to reduce Nitrogen, Phosphorous and Heavy Metal Availability, *Journal of Soil Contamination*, Vol. 7, (1998), 191-212.
23. V. Feigel et al., Red Mud as a Chemical Stabilizer for Soil Contaminated with Toxic Metals, *Water, Air & Soil Pollution*, Vol. 223, (2012), 1237-1247.
24. W. Friesl, O Horak and WW Wenzel, Immobilization of heavy metals in soils by the application of bauxite residues: pot experiments under field conditions, *Journal of Plant Nutrition Soil Science*, Vol. 167, (2004), 54-59.
25. C.W. Gray et al., Field evaluation of in situ remediation of a heavy metal contaminated soil using lime and red mud, *Environmental Pollution*, Vol. 142, (2006), 530-539.
26. Z. Jiang, C Liu and L Sun, Catalytic Properties of Silver Nanoparticles Supported on Silica Spheres, *Journal of Physical Chemistry Biology*, Vol. 109, (2005), 1730-1735.
27. F.U. Khan et al., Antioxidant and catalytic applications of silver nanoparticles using Dimocarpus logan seed extract as a reducing and stabilizing agent, *Journal of Photochemistry and Photobiology B: Biology*, Vol. 164, (2016), 344-351.
28. J. Saha et al., A novel green synthesis of silver nanoparticles and their catalytic action in reduction of Methylene Blue dye, *Sustainable Environment Research*, Vol. 27, (2017), 245-250.
29. F. Ni et al., Preparation of coagulant from red mud and semi-product of polyaluminium chloride for removal of phosphate from water, *Desalination and Water Treatment*, Vol. 40, (2012), 153-158.
30. Y. Du et al., Fabrication of a low-cost adsorbent supported zero-valent iron by using red mud for removing Pb (II) and Cr (VI) from aqueous solutions, *RSC Advanced*, Vol 9, (2019), 33486-33496.
31. H. Genç et al., Adsorption of arsenate from water using neutralized red mud, *Journal of Colloid and Interface Science*, Vol. 264, (2003), 327-334.
32. Y. Cui et al., Cr (VI) Adsorption on Red Mud Modified by Lanthanum: Performance, Kinetics and Mechanisms, *PLoS ONE*, Vol. 11, (2016).
33. S.S. Prajapati, PAM Najar and VM Tangde, Removal of Phosphate Using Red Mud: An Environmentally Hazardous Waste By-Product of Alumina Industry, *Advances in Physical Chemistry*, Vol. 12, (2016), 1-9.
34. P. Vachon et al., Chemical and biological leaching of aluminium from red mud, *Environmental Science & Technology*, Vol. 28, (1994), 26-30.
35. A. Gök, M Omastová and J Prokeš, Synthesis and characterization of red mud/polyaniline composites: Electrical properties and thermal stability, *European Polymer Journal*, Vol. 43, (2007), 2471-2480.
36. B. Khodashenas and HR Ghorbani, Synthesis of silver nanoparticles with different shapes, *Arabian Journal of Chemistry*, Vol. 12, (2019), 1823-1838.
37. L. Yanget et al., High Efficient Photocatalytic Degradation of p-Nitrophenol on a unique Cu_2O/TiO_2 p-n Heterojunction Network Catalyst, *Environmental Science & Technology*, Vol. 44, (2010), 7641-7646.
38. C. Borrás et al., Study of the oxidation of solutions of p-chlorophenol and p-nitrophenol on Bi-doped PbO_2 electrodes by UV-Vis and FTIR in situ spectroscopy, *Electrochimica Acta*, Vol. 49, (2004), 641-648.
39. C.M. Friend and B Xu et al., Heterogeneous Catalysis: A Central Science for a Sustainable Future, *Accounts of Chemical Research*, Vol. 50, (2017), 517-521.
40. M.A. Khairul et al., The composition, recycling and utilisation of Bayer red mud, *Resources, Conservation and Recycling*, Vol. 141, (2019), 483-498.
41. W. Hajjaji et al., Composition and technological properties of geopolymers based on metakaolin and red mud, *Materials & Design*, Vol. 52, (2013), 648-654.
42. B. Hallac et al., In Situ UV -Visible Assessment of Iron-Based High-Temperature Water-Gas Shift Catalysts Promoted with Lanthana: An Extent of Reduction Study, *Catalysis*, Vol. 8, (2018), 63.

43. R.A. Schoonheydt, UV-VIS-NIR spectroscopy and microscopy of heterogeneous catalysts, *Chemical Society Reviews*, Vol. 39, (2010), 5051.
44. N. Kimura, W Kitagwa and Y Kamagata, A novel p-nitrophenol degradation gene cluster from a gram-positive bacterium, Rhodococcus opacus, *Journal of Bacteriology*, Vol. 15, (2004), 4894-4902.
45. N. Pradhan, A Pal and T Pal, Catalytic Reduction of Aromatic Niro Compounds by Coinage Metal Nanoparticles, *Langmuir*, Vol. 17, (2001), 1800-1802.
46. X. Wang et al., Catalytic degradation of PNP and stabilization/solidification of Cd simultaneously in soil using microwave-assisted Fe-bearing attapulgite, *Chemical Engineering Journal*, Vol. 304, (2016), 747-756.
47. I. Koehne et al., Synthesis and Structure of Six-Coordinate Iron Borohydride Complexes Supported by PNP Ligands, *Inorganic Chemistry*, Vol. 52, (2014), 2133-2143.
48. M.S. Samuel et al., Biosynthesized silver nanoparticles using Bacillus amyloliquefaciens; Application for cytotoxicity effect on A549 cell line and photocatalytic degradation of p-nitrophenol, *Journal of Photochemistry and Photobiology B: Biology*, Vol. 202, (2020), 111-642.
49. M. Nekoeiniaet et al., Highly efficient catalytic degradation of p-nitrophenol by Mn_3O_4/CuO nanocomposite as a heterogeneous fenton-like catalyst, *Journal of Experimental Nanoscience*, Vol. 15, (2020), 322-336.
50. Z. Xiong et al., Degradation of p-nitrophenol (PNP) in aqueous solution by a micro-size FeO/O_3 process: Optimization, kinetic, performance and mechanism, *Chemical Engineering Journal*, Vol. 302, (2016), 137-145.